By comparing Eqs. (11) and (12), we now find

$$\frac{\gamma}{U} = \frac{2\phi}{U^2} \tag{13}$$

Thus, by Eqs. (9, 10, and 13)

$$\frac{\gamma}{U} = 2(2k_{\dot{\alpha}} - k_{\dot{v}})\sin\theta + \frac{2C}{U^2}\tan\frac{\theta}{2} \tag{14}$$

where by definition

$$k_{\dot{\alpha}} = \frac{\dot{\alpha}c}{2U} \tag{15}$$

$$k_{\dot{v}} = \frac{(-\dot{U}/U)\alpha c}{2U} \tag{16}$$

The first term on the right-hand side of Eq. (14) is recognized as being the vortex distribution of a parabolic arc meanline which is symmetric about the midchord, and whose ideal angle of attack therefore is zero. The second term on the right-hand side is the vortex distribution of a flat plate airfoil at angle of attack. The constant C determines the lift lag of the additional distribution in unsteady flow. This constant can be found by applying the boundary condition at the airfoil surface, making use of the Cauchy-Riemann condition, and performing an integration. This will not be done here, since it is believed that the lag is insignificant for all cases of practical interest to maximum lift. Note that there is no lift lag for the effective camber change of the airfoil.

The effective camber η_c may be found by substituting Eq. (14) into the following expression from thin airfoil theory, and integrating.

$$\frac{d\eta_c}{d\bar{x}_0} = (1/2\pi)\int_{-c/2}^{c/2} \frac{(\gamma/U)}{\bar{x} - \bar{x}_0}\, d\bar{x} \tag{17}$$

The result is

$$\eta_c/c = (2k_{\dot{\alpha}} - k_{\dot{v}})[(1/4) - (\bar{x}/c)^2] \tag{18}$$

From thin airfoil theory it is also known that the angle for zero lift α_{ZL} of a parabolic meanline is equal to twice the maximum camber, i.e.,

$$-\alpha_{ZL} = k_{\dot{\alpha}} - \tfrac{1}{2}k_{\dot{v}} \tag{19}$$

Unsteady flow of the type investigated here will therefore yield a lift coefficient increase ΔC_L at a given angle of attack in the linear region as follows:

$$\Delta C_L = 2\pi(k_{\dot{\alpha}} - \tfrac{1}{2}k_{\dot{v}}) \tag{20}$$

At least part of this change might be expected to affect the maximum lift coefficient, indicating an increase due to rate of change of angle of attack and a decrease due to deceleration. However, the reader may easily convince himself that the predicted ΔC_L change due to inviscid flow conditions is negligible compared to the test results obtained, both for jet transports and also for helicopter rotor blades. It is concluded that the measured large increases in maximum lift coefficients in unsteady flow are associated with boundary-layer phenomena, rather than being caused by the inviscid flow.

References

[1] Kier, D. A., "Flight Comparison of Several Techniques for Determining the Minimum Flying Speed for a Large, Subsonic Jet Transport," TN D-5806, June 1970, NASA.

[2] Biot, M. A., "Some Simplified Methods in Airfoil Theory," *Journal of the Aeronautical Sciences*, Vol. 9, March 1942, pp. 186–190.

[3] Wood, J. E., "Application of the Acceleration Potential to Aerodynamic Force Calculation in Oscillating Flow," M. S. thesis, Dept. of Aeronautics June 1970, Naval Postgraduate School, Monterey, Calif.

Evaluation of Reissner's Correction for Finite Span Aerodynamic Effects

B. K. DONALDSON*
The Boeing Company, Wichita, Kansas

REFERENCES 1 and 2 set forth Reissner's method for calculating the effect of finite span upon the unsteady airloads acting upon an harmonically oscillating wing. Reissner's method is limited to incompressible flow, but it is applicable to any wing planform, at least down to an aspect ratio of three. An advantage of the Reissner theory is that it is only a modification of basic strip theory,[3] which simplifies its application. In addition, the calculations required by the Reissner method are less extensive than those required by lifting surface theory. The accuracy of the Reissner method is the concern of this Note. To evaluate that accuracy, the Reissner method was applied to ten moderate-aspect-ratio model wings. The Reissner flutter speeds that were the result of those analyses are compared to experimental flutter speeds obtained from repeated wind-tunnel testing, and also to basic strip theory results.

The ten model wings which are the subjects of the analyses were all of sufficiently low aspect ratio that finite span effects were significant. The model wing geometries, mass distributions, and stiffness distributions were typical of actual wing construction. Each semispan model had a planform area of 1620 in.^{2} A typical semispan length was 37.65 in. This size permitted good precision in measuring model parameters. With one exception, each model wing represented a single variation in the geometric design parameters of aspect ratio, thickness ratio, taper ratio, and leading-edge sweepback angle. Thus, the wind tunnel data is an indication of the effect of these wing parameters on flutter speed. See Table 1. The high speed wings, for which these were models, were designed for the same airplane. Each wing required a different tail loading, so each wing was designed to have the necessary strength to support a particular wing loading. As a consequence of this and the different configurations, the model wings had different stiffness and mass properties.

Because of their single-spar, weighted-segment-type construction, these models were well suited for a structurally simple evaluation of unsteady airload theories. Each wing spar supported nine lead weighted, balsa wood panels whose width was one-tenth of the semispan length. An additional inboard panel was fixed to the fuselage support from which the wings were cantilevered. Each of the nine outboard panels was fixed on the spar at the panel midpoint, except for the most outboard panel which, for different models, was fixed at varying, more inboard points. There was no elastic interaction between panels other than that provided by the single spar. Thus, an elastic-axis, discrete-mass mathematical description of the model wings was entirely appropriate. The ratios of the spar area moments of inertia were such that just three degrees-of-freedom were indicated for each wing panel: vertical bending deflection, bending slope angle, and torsional twist. The center of gravity locations, first mass moments, moments of inertia, and product of inertia were carefully measured or estimated for each panel. The spar stiffness design data were corrected by experimental deflection

Received February 2, 1972; revision received April 10, 1972. The author would like to thank L. J. Topp for general guidance, and D. Fall, G. Wells, and J. Symes, of the Boeing Co. for assistance with the calculations. The experimental work was supervised by G. Luessen of the Boeing Co. The author would also like to thank H. Ashley, University of Maryland, for discussing this Note.

Index category: Aeroelasticity and Hydroelasticity.

* Structural Dynamics Engineer, Structural Dynamics Unit. Presently Assistant Professor, University of Maryland, College Park, Md. Member AIAA.

Table 1 Model wing geometry, flutter speed, and flutter frequency results

Wing no.	A.R.[a]	%TH.[b]	T.R.[c]	Λ[d]	Wind-tunnel results Speed, mph	Wind-tunnel results Freq., Hz	Basic strip theory Speed, mph	Basic strip theory %Test speed	Basic strip theory Freq., Hz	Reissner's Theory Speed, mph	Reissner's Theory %Test speed	Reissner's Theory Freq., Hz
1	3.5	3.5	0.2	45°	95.9	12.5	68.9	71.8	14.53	99.61	103.9	11.97
2	3.5	2.5	0.2	45°	76.2	10.62	47.41	62.2	11.15	65.55	86.0	10.44
3	3.5	4.5	0.2	45°	107.0	14.7	86.11	80.5	15.72	105.02	98.1	13.67
4	2.5	3.5	0.2	45°	92.4	14.86	73.01	79.1	13.57	92.56	100.2	13.28
5	4.5	3.5	0.2	45°	88.3	13.25	62.45	70.7	12.51	83.27	94.3	11.77
6	4.5	4.5	0.2	45°	111.9	16.67	80.18	71.7	14.68	105.53	94.3	13.08
7	3.5	3.5	0.2	30°	92.7	12.5	75.04	80.9	11.55	90.77	97.9	11.42
8	3.5	3.5	0.2	55°	102.1	12.5	65.81	64.5	11.18	90.33	88.5	8.79
9	3.5	3.5	0.1	45°	92.2	14.3	78.29	84.9	15.37	91.80	99.6	14.06
10	3.5	3.5	0.3	45°	91.6	12.2	71.32	77.9	10.03	86.29	94.2	9.36

[a] Wing aspect ratio.
[b] Percent thickness.
[c] Taper ratio.
[d] Sweepback angle along leading edge.

data. The success of the mathematical description of the model wing inertia and elastic properties is discussed below in the discussion of the vibration analyses data.

The model wings were also in keeping with the assumption of the airload theories. The streamwise panels were thin and of symmetric thickness. The model wings were mounted on the wind-tunnel ceiling at zero angle-of-attack. They were dynamically scaled to flutter well within the incompressible regime. The only possible difficulty was that the taper ratios were not moderate. For the sake of simplicity, all of the models were without control surfaces. Further information on the models, and the vibration and flutter analyses discussed below can be found in Ref. 4.

Vibration tests were conducted for each of the model wings. Their zero airspeed natural frequencies were obtained, but it proved impossible to obtain the mode shapes without unacceptable distortion. Therefore, to obtain mode shape information, vibration analyses were performed. The frequency results of those analyses are shown in Table 2. Disregarding the unimportant fifth mode, the analytical frequency results are reasonably good. Allowance must be made for the fact that the test results must differ from the theoretical results because of the frequency reducing effects of the additional effective mass of the ambient air, and the added mass of the test shaker coils. These effects combined were estimated to be sufficient to cause as much as a 2% or 3% variation in the lower modes, and slightly more in the higher modes. In all cases there were no significant disagreements between the qualitative descriptions of the experimental natural mode shapes and the descriptions of the calculated mode shapes. Therefore, the results of the vibration analyses were considered suitable for the flutter analyses.

As mentioned previously, two sets of flutter analyses were performed. In both the basic strip theory analyses and the finite span analyses, a flutter determinant equation was solved by choosing values of the reduced frequency and solving for both the damping necessary for neutral stability and the flutter frequency. As a conservative measure, zero structural damping was assumed. Therefore the flutter speed was the airspeed at which the equivalent aerodynamic damping was zero. In both sets of flutter analyses, the effect of sweepback on the unsteady airloads was accounted for by introducing as a factor the cosine of the quarterchord sweepback angle (see Ref. 5, p. 395). In both sets of flutter analyses, the quarterchord vertical deflections and streamwise angles of attack at the panel midpoints were represented by the weighted sum of the five quarterchord mode shapes. The quarterchord mode shapes were calculated from the elastic axis mode shapes through a coordinate transformation that assumed no chordwise bending. Since the panels had stiff metal bracing between the quarterchord and the three-quarterchord, this was a valid assumption. Since the finite span correction functions depend on the wing deflection shape as well as the local reduced frequency, the use of coupled modes in the finite span flutter analyses meant that a correction function for vertical deflection and another for streamwise angular deflection had to be calculated for each of the natural modes. Since, as Reissner pointed out, the finite span airloads are those of two-dimensional basic strip theory altered by adding appropriate finite span corrections to Theodorsen's function $C(k)$ it was necessary to meet the requirement of associating the proper correction function with its corresponding deflection. To accomplish this, the finite span airloads matrix was written as the sum of the basic strip theory matrix in modal coordinates and a finite span correction matrix for each mode which was multiplied by the corresponding modal amplitude vector and the modal coordinate. Thus, the coupling between modes in both the case of the basic strip theory

Table 2 Comparison of test and calculated natural frequencies (Hz)

Wing no.	First mode Test	First mode Calc.	First mode %diff.	Second mode Test	Second mode Calc.	Second mode %diff.	Third mode Test	Third mode Calc.	Third mode %diff.	Fourth mode Test	Fourth mode Calc.	Fourth mode %diff.	Fifth mode Test	Fifth mode Calc.	Fifth mode %diff.
1	4.51	4.616	+2½	12.26	12.459	+2½	17.92	18.579	+3½	21.02	22.548	+7½	30.56	29.369	−4
2	3.51	3.526	+½	9.01	9.357	+4	13.66	14.292	+4½	15.63	16.426	+5	21.54	21.024	−2½
3	5.47	5.579	+2	14.15	14.228	+½	20.63	21.744	+5½	23.51	25.178	+7	34.26	34.313	+0
4	6.85	7.011	+2½	17.1	17.459	+2	17.68	18.669	+5½	26.5	27.668	+4½	28.3	32.565	+15
5	3.30	3.328	+1	8.40	8.520	+1½	15.54	16.000	+3	18.00	18.794	+4½	25.89	24.073	−7
6	3.79	3.871	+2	9.62	10.127	+5½	18.15	19.292	+6½	22.82	22.812	−0	33.3	29.910	−10
7	5.56	5.728	+3	15.00	16.154	+7½	16.22	17.000	+5	24.19	24.938	+3	27.08	31.891	+18
8	3.27	3.296	+1	8.06	8.302	+3	14.13	14.578	+3	17.78	18.480	+4	24.19	21.609	−12
9	4.78	4.895	+2½	12.2	12.779	+5	18.75	20.303	+8½	21.95	23.336	+6½	28.00	31.190	+11½
10	4.40	4.465	+1½	11.05	11.163	+1	16.25	15.913	−2	18.30	19.684	+7½	24.31	25.915	+6½

airloads and the case of the finite span airloads arises only when the unsteady lifts and moments are used to calculate the generalized (modal) forces. At this point note, of course, that the basic strip theory analyses were the same as the finite span analyses, but with the finite span correction matrices omitted.

There was a second variation in style from the procedure for calculating the finite span airloads outlined on pp. 14 and 15 of Ref. 2. The tables of Ref. 2 are set up for calculating the finite span unsteady airloads at every two-tenths of the semispan. In the case of the model wings, there would only be five points of definition for the airloads, and the airloads would be based on only a five point description of the natural modes. Since p. 1 of Ref. 2 states "...the effect of finite span depends appreciably on the shape of the wing deflection functions," and since the modal amplitudes would have been poorly described by just a five point definition, the author decided to abandon the tables of Ref. 2 and retain the nine point definitions of the mode shapes. Thus the unsteady airloads were calculated with better accuracy at their natural locations, i.e., the midpoints of the panel quarterchords. The price that had to be paid for this decision was the necessity for calculating the Reissner functions $S_n(k_o s,\phi_i)$ defined in Ref. 2 where n is a series index number, $k_o s$ is a reduced frequency referenced to the semispan length, and $\cos\phi_i$ is a nondimensional spanwise coordinate. The complex values of the functions S_n are difficult to calculate because those values depend upon an integral involving Cicala's function (see Ref. 2, p. 37). While the imaginary portion of Cicala's function presents no difficulty on a finite interval, the real part is unbounded as the argument approaches zero. This produces a discontinuity in the integrand of the imaginary part of S_n, such that at values of the variable of integration slightly less than the value at the point of discontinuity, the integrand logarithmically approaches plus infinity, while at values of the variable of integration slightly greater than that at the point of discontinuity, the integrand logarithmically approaches minus infinity. This integrand was integrated on a digital computer by using straight line interpolation along with the values of Cicala's function tabulated in Ref. 2 down to an argument value of 0.05. For lesser values of the Cicala function argument, it was assumed that the sharp rise in opposite directions produced a zero net value for the integral across the discontinuity. This questionable assumption was investigated by reproducing three of the four S_n tables that appear in Ref. 2. Generally there was good agreement, but there were also points of disagreement. The disagreements were mostly among the more difficult imaginary parts, but it is significant that they also occurred among the real parts. For example, the real part of S_7 (2, arccos 0.2) from Ref. 2 is -0.299. A hand calculation using a polynomial approximation presented in Ref. 2 yielded the value -0.1269. A desk top sized graphical solution produced -0.1273, and the digital computer program gave -0.1250. Here the computer program, as opposed to the tables of Ref. 2, is clearly favored. A case that was not quite as clear was the imaginary portion of S_5 (2, arccos 0.8). The table of Ref. 2 says $+0.115$; a desk top sized graph said $+0.0175$; and the computer said $+0.0051$. The final justification for the use of the digital computer values of S_n can only be the reasonable calculated flutter airspeeds that were obtained. See Table 1.

The flutter airspeed results indicate a marked improvement in analytical accuracy when the Reissner theory results are contrasted to the basic strip theory results. In two of the ten cases, however, the finite span solutions were slightly nonconservative. The basic strip theory results evidenced their usual wide range of conservativeness. Thus it, would appear that having both types of results would be useful. All that can be said for the flutter frequency results is that the Reissner theory values are less than the wind-tunnel values. Graphs of this small number of data points indicate the that Reissner solutions follow the experimental trends for variations in aspect ratio, taper ratio and thickness ratio. At the high sweepback angle of 55°, however, the trends were opposite.

References

[1] Reissner, E., "Effect of Finite Span on the Airload Distributions for Oscillating Wings, Part 1: Aerodynamic Theory of Oscillating Wings of Finite Span," TN 1194, March 1947, NACA.

[2] Reissner, E. and Stevens, J. E., "Effect of Finite Span on the Airload Distributions for Oscillating Wings, Part II: Methods of Calculation and Examples of Application," TN 1195, Oct. 1947, NACA.

[3] Theodorsen, T. and Garrick, I. E., "Nonstationary Flow About a Wing-Aileron-Tab Combination Including Aerodynamic Balance," TR 736, 1942, NACA.

[4] Donaldson, B. K., "An Evaluation of the Reissner Finite Span Correction Functions," M.S. thesis, 1963, Wichita State Univ., Wichita, Kansas.

[5] Bisplinghoff, R. E., Ashley, H., and Halfman, R. L., *Aeroelasticity*, 1st ed., Addison-Wesley, Reading, Mass., 1955.

Drag of a Flat Plate with Transition in the Absence of Pressure Gradient

CHANG-YU LIU*
Chung Shan Institute of Science and Technology, Lung-Tan, Taiwan, Republic of China

Introduction

BASED on a more sound analysis than Schlichting's[1] formula, Collar[2] obtained a closed formula for the drag of a flat plate with transition in the absence of pressure gradient But Collar's formula gives no better agreement with existing data than the Schlichting formula. The present Note shows that, if the logarithmic skin-friction relation is used instead of the skin-friction relation deduced from the $\frac{1}{7}$th power law velocity distribution, a better agreement can be obtained.

Analysis

Similar to the analysis given by Collar, Fig. 1 shows the model. X_c is the transition point and X_i is the notional leading edge of a plate which in wholly turbulent flow gives an identical turbulent layer from X_c to L. Assuming that the turbulent layer from X_i to X_c follows the $\frac{1}{7}$th power law and the momentum thickness is continuous at X_c, we have

$$0.664(\nu X_c/U)^{1/2} = 0.036(X_c - X_i)\{[U(X_c - X_i)]/\nu\}^{1/5} \quad (1)$$

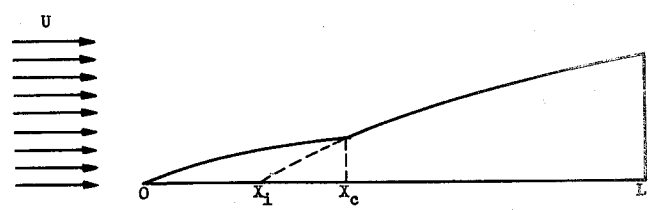

Fig. 1 The model.

Received April 10, 1972.
Index category: Airplane and Component Aerodynamics.
* Associate Scientist.